A Wideband X/Ku/Ka-band SATCOM 8-Channel SiGe Transmit Beamformer Chip in a 16-Element Phased-Array

Oguz Kazan, Zhaoxin Hu, Abdulrahman Alhamed, and Gabriel M. Rebeiz
University of California, San Diego, La Jolla, CA, USA
okazan@ucsd.edu, z1hu@ucsd.edu, aalhamed@ucsd.edu, grebeiz@ucsd.edu

***Abstract*—This paper presents a 5-33 GHz 8-channel transmit beamformer implemented in 90nm SiGe BiCMOS HBT technology. Each channel is composed of a wideband two-stage power-amplifier (PA), a phase-shifter (PS), a variable gain amplifier (VGA) and single-ended to differential converter (S2D). The input RF power is distributed to the 8-channels using a two-stage Wilkinson network and active dividers. The measured small-signal gain is 24-27 dB at 5-33 GHz with 5-bit phase-shifter operation and > 20 dB gain control. A peak OP1dB and OPsat of 13-14 dBm is achieved at Ku-band. The beamformer is attached to a 16-element wideband antenna array and shows scanning performance at 8-30 GHz. To author's knowledge, this work achieves the widest bandwidth Tx beamforming chip. Application areas are ground terminals capable of communications with X, Ku and Ka-band satellite constellations.**

***Keywords*—phased-array, SATCOM, wideband, PA, SiGe HBT.**

I. Introduction

Current SATCOM systems enable high data rate and low latency communications with low Earth-orbit (LEO) and medium Earth-orbit (MEO) satellites. However, there are multiple frequencies used, from X-band (8 GHz), Ku-band (14 GHz) and Ka-band (29 GHz) (Fig.1a). A ground terminal which covers all satellite bands in a single system simplifies the hardware complexity, allows for worldwide operation over multiple providers, and reduces the overall terminal cost.

This paper presents an 8-channel transmit (Tx) beamformer designed in a 90nm SiGe BiCMOS technology. The design covers the X, Ku and Ka SATCOM bands in a single chip for next-generation phased-array systems. The 8-channel chip is compact and fits well in a 31 GHz phased-array design based on the 2x2 (quad-antenna) approach [1]. It is also proven in a 16-element phased-array.

II. Eight-Channel Wideband Beamformer

Fig.1b presents a block diagram of the wideband 8-channel Tx beamformer. The input power is distributed to the channels using a wideband two-section Wilkinson network, followed by a single-ended to differential converter. The channels are all differential and contain a wideband VGA, a 5-bit phase shifter and a wideband power amplifier. The outputs are also differential which improves the stability over a wide frequency range. Also, wideband antennas are differential in nature, and differential output ports eliminate the use of wideband baluns and result in a more efficient system.

The chip is implemented in the Tower Semiconductor 90nm SiGe BiCMOS process with 7 aluminum metal layers.

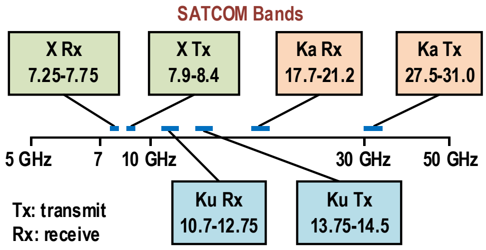

(a)

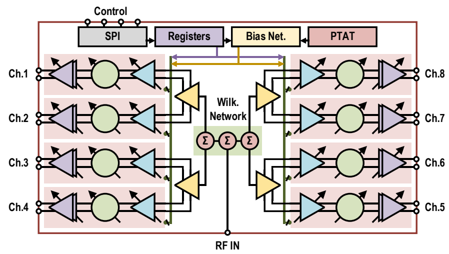

(b)

Fig. 1. (a) X, Ku and Ka-band SATCOM frequencies for commercial and defense systems. (b) Block diagram of the wideband 8-channel Tx beamformer chip.

The top two metal layers are used for high Q inductors (Q ~16 at 25 GHz). The simulated fT and fmax of a 3um emitter length HBT is 245 GHz and 304 GHz, respectively.

A. Wilkinson Network

The input power is distributed using a 1:4 Wilkinson network with two-section Wilkinson-dividers to increase the bandwidth (Fig.1b). The 1:4 divider network insertion loss (ohmic loss) is 1.8-3.8 dB at 5-33 GHz and does not include the 6 dB division loss. The increase in the insertion loss is compensated by increasing the channel gain at high frequencies, resulting in a nearly flat response.

B. Active Phase Shifter

The active phase shifter employs a vector modulator architecture with a quadrature all-pass filter (QAF) (Fig. 2). The I/Q signals are fed to two variable gain amplifiers with current-steering, and the output signals are added in the current mode. For wideband operation, de-Q series resistors are used for the inductors and the capacitors in the QAF network [2-5]. The QAF network is followed by an LC compensation network to introduce a nearly resistive interface to the VGAs. The phase shifter has simulated small-signal gain of 1.6-4.5 dB and a NF of 8.4-11 dB at 5-33 GHz. An I/Q error of up to 2.2 dB and 8.3° is present over the entire bandwidth, which is relatively high. Therefore, a 6^{th} bit is employed in the VGA current steering to compensate for the I/Q error, and this results in true 5-bit operation at 5-33 GHz

This paper's copyright is held by the author(s). It is published in these proceedings and included in any archive such as IEEE Xplore under the license granted by the "Agreement Granting EurAAP Rights Related to Publication of Scholarly Work."
Authorized licensed use limited to: Seoul National University. Downloaded on March 18,2024 at 05:39:21 UTC from IEEE Xplore. Restrictions apply.

(different 32 phase shifter states chosen for different frequency bands).

The two-stage power amplifier has a simulated small-signal gain of 27.3-24.7 dB at 5-33 GHz, and a OP1dB of 10-13.4 dBm. The PA consumes 76.8 mW from a 2.4 V supply, resulting in a PAE of 13-25% at 5-33 GHz.

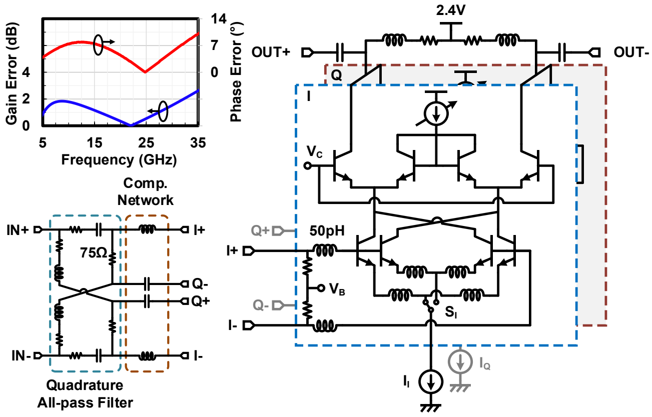

Fig. 2. Wideband vector-modulator phase shifter and the QAF network with the simulated I/Q magnitude and phase error.

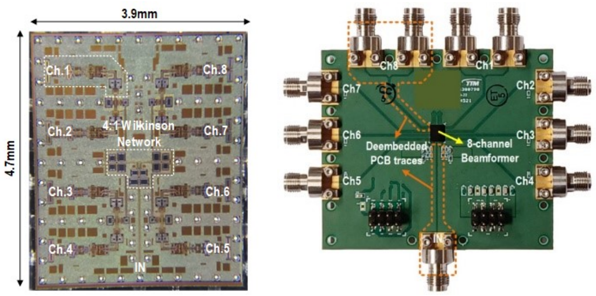

Fig. 3. Die photo of the 8-channel Tx beamformer chip and PCB for beamformer evaluation. Some ports are differential all the way to the connectors and some ports are (half) terminated by 50 Ω and taken as single ended to the connectors.

III. MEASUREMENTS

Measurements are done on a packaged chip and not on-wafer. The beamformer die photo is shown in Fig. 3. The chip size is 3.9x4.7 mm^2. The PCB trace and connector losses are de-embedded, and the reference planes are at the chip input and output ports (on the PCB). The chip consumes 1.8 W with a 2.4 V supply at small signal. The power increases to 1.9 W at P1dB resulting in 240 mW per channel.

Fig. 3a presents the electronic gain of the 8-channel beamformer. The maximum electronic gain is 27.4 dB with the 3-dB bandwidth of 5-33 GHz, and all channels are within +/-1 dB of each other. The gain control is shown in Fig. 3b. The VGA and DPA (driver for the PA) have 15 dB and 6 dB gain control, respectively, resulting in 21 dB of gain control. Fig. 3c presents the measured phase performance. The 6-bit performance is trimmed to 32 states at 8 GHz, 14 GHz and 30 GHz, and the rms phase error is plotted. One can see that 5-bit operation is achieved with an RMS error of < 5.2° for each setting. The RMS amplitude error is ~1 dB for each case. The beamformer chip delivers a peak P1dB of 13.1 dBm at 14 GHz. The beamformer delivers a maximum of 14.7 dBm OPsat at 14 GHz.

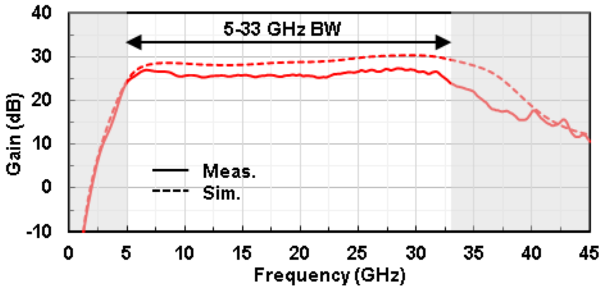

(a)

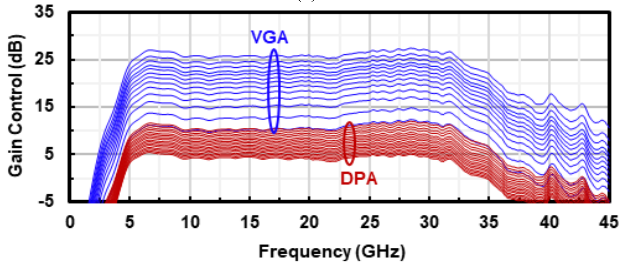

(b)

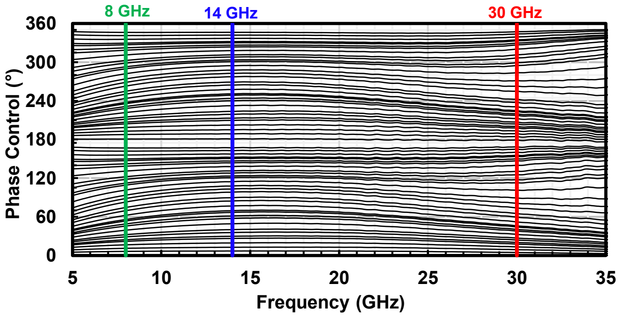

(c)

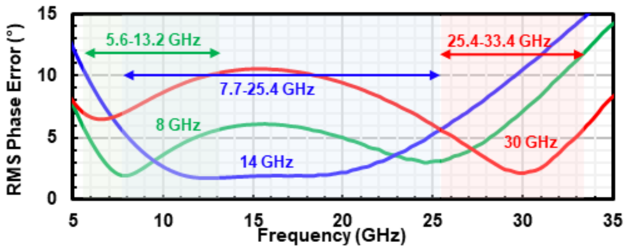

(d)

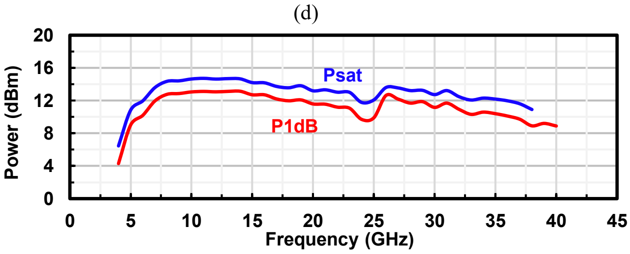

(e)

Fig. 3. (a) Electronic gain, (b) Gain control, (c) Phase control, (d) Large-signal performance.

This paper's copyright is held by the author(s). It is published in these proceedings and included in any archive such as IEEE Xplore under the license granted by the "Agreement Granting EurAAP Rights Related to Publication of Scholarly Work."
Authorized licensed use limited to: Seoul National University. Downloaded on March 18,2024 at 05:39:21 UTC from IEEE Xplore. Restrictions apply.

In the next step, two beamformer chips are attached to a 16-element wideband tapered slot antenna array on a low-cost PCB (printed circuit board) as shown in Fig. 4. The slot antennas are differentially-fed from the 8-chip ports, and an input 3-stage Wilkinson network is used on the PCB to feed the two chips. The array is then calibrated at 8 GHz, 14 GHz, 21 GHz and 30 GHz by measuring S21 in the far field and using the phase and amplitude control on each channel to compensate for the differences between the different channels. The measured patterns show excellent performance up to 24 GHz, but due to the thickness of the substrates, the antennas did not scan well at 30 GHz.

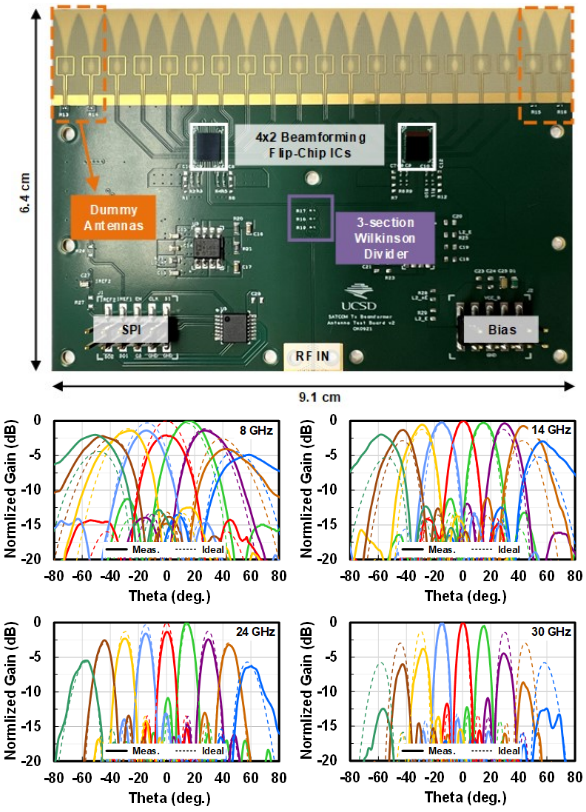

Fig. 4. Fabricated 16-element array using two beamformer chips and measured scanned patterns at 8 GHz, 14 GHz, 24 GHz and 30 GHz.

The measured EIRP is shown in Fig. 5 and agrees well with simulations. The simulated EIRP takes into account the output power, the antenna gain and the loss between the antennas and the beamformer chip. Good agreement is obtained.

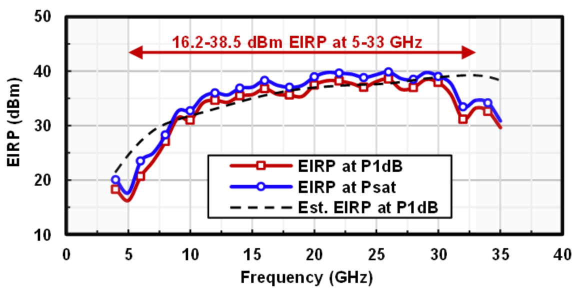

Fig. 5. Measured and simulated EIRP vs. frequency at broadside. This is done in the far filed with calibration every 5 GHz.

IV. Conclusion

An ultra-wideband 8-channel Tx beamformer is presented. The channels employ a differential architecture with 5-bit of phase control and high OP1dB. This work is intended for phased array systems operating at multiple SATCOM bands and its operation is demonstrated on a 16-element linear tapered-slot antenna array.

Acknowledgment

This work was supported by the MITRE Corporation.

References

[1] L. D. Earley, "Communication in Challenging Environments: Application of LEO/MEO Satellite Constellation to Emerging Aviation Networks," *2021 Integrated Communications Navigation and Surveillance Conference (ICNS)*, 2021, pp. 1-8, doi: 10.1109/ICNS52807.2021.9441549.

[2] M. Sayginer and G. M. Rebeiz, "An Eight-Element 2–16-GHz Programmable Phased Array Receiver With One, Two, or Four Simultaneous Beams in SiGe BiCMOS," in *IEEE Transactions on Microwave Theory and Techniques*, vol. 64, no. 12, pp. 4585-4597, Dec. 2016, doi: 10.1109/TMTT.2016.2620144.

[3] K. Kibaroglu, M. Sayginer and G. M. Rebeiz, "A Low-Cost Scalable 32-Element 28-GHz Phased Array Transceiver for 5G Communication Links Based on a 2x2 Beamformer Flip-Chip Unit Cell," in *IEEE Journal of Solid-State Circuits*, vol. 53, no. 5, pp. 1260-1274, May 2018, doi: 10.1109/JSSC.2018.2791481.

[4] A. Alhamed, G. Gültepe and G. M. Rebeiz, "A Multi-Band 16-52-GHz Transmit Phased Array Employing 4 x 1 Beamforming IC With 14-15.4-dBm Psat for 5G NR FR2 Operation," in *IEEE Journal of Solid-State Circuits*, doi: 10.1109/JSSC.2021.3134325.

[5] A. Khalil et al., "2.1 mm-Wave 5G Radios: Baseband to Waves," *2021 IEEE International Solid- State Circuits Conference (ISSCC)*, 2021, pp. 38-40, doi: 10.1109/ISSCC42613.2021.9365980.

This paper's copyright is held by the author(s). It is published in these proceedings and included in any archive such as IEEE Xplore under the license granted by the "Agreement Granting EurAAP Rights Related to Publication of Scholarly Work."

Authorized licensed use limited to: Seoul National University. Downloaded on March 18,2024 at 05:39:21 UTC from IEEE Xplore. Restrictions apply.